Effects of channel cross-sectional geometry on long wave generation and propagation

Michelle H. Teng
Department of Civil Engineering, University of Hawaii at Manoa, Honolulu, Hawaii 96822

Theodore Y. Wu
Engineering Science, California Institute of Technology, Pasadena, California 91125

(Received 3 February 1997; accepted 15 July 1997)

Joint theoretical and experimental studies are carried out to investigate the effects of channel cross-sectional geometry on long wave generation and propagation in uniform shallow water channels. The existing channel Boussinesq and channel KdV equations are extended in the present study to include the effects of channel sidewall slope at the waterline in the first-order section-mean equations. Our theoretical results show that both the channel cross-sectional geometry below the unperturbed water surface (characterized by a shape factor κ) and the channel sidewall slope at the waterline (represented by a slope factor γ) affect the wavelength (λ) and time period (T_s) of waves generated under resonant external forcing. A quantitative relationship between λ, T_s, κ, and γ is given by our theory which predicts that, under the condition of equal mean water depth and equal mean wave amplitude, λ and T_s increase with increasing κ and γ. To verify the theoretical results, experiments are conducted in two channels of different geometries, namely a rectangular channel with $\kappa \equiv 1$, $\gamma = 0$ and a trapezoidal channel with $\kappa = 1.27$, $\gamma = 0.16$, to measure the wavelength of free traveling solitary waves and the time period of wave generation by a towed vertical hydrofoil moving with critical speed. The experimental results are found to be in broad agreement with the theoretical predictions. © *1997 American Institute of Physics.* [S1070-6631(97)03211-X]

I. INTRODUCTION

Natural and man-made water channels often have non-rectangular cross sections. It is important to understand how channel geometry affects the evolution of long waves in water channels of arbitrary shape. Previous studies have shown that when a long wave propagates in a shallow water channel, the wave profiles in both the lateral and longitudinal directions are affected by the channel cross-sectional geometry. For example, a long wave traveling in a channel with sloping sidewalls exhibits a noticeable variation in wave amplitude along the lateral direction, whereas in a rectangular channel, the wave height is uniform across the channel. In a channel with walls fanning outwards, the wave height is found to increase monotonically from its lowest elevation at the channel centerline to reach its highest climb at the sloping bank. This phenomenon was reported by Russell,[1] and Sandover and Taylor,[2] and was further investigated both theoretically and experimentally by Peregrine[3,4] whose theory provided an analytical description of the lateral wave variation in non-rectangular channels.

Theoretical results from Peters'[5] and Peregrine's[3] studies also revealed another important aspect, namely the effect of channel geometry on the wave profile in the longitudinal direction. It was shown that, for waves traveling in a uniform non-rectangular channel whose sidewalls are vertical or close to vertical at the waterline, the equations describing the mean wave in a non-rectangular channel can be converted to that for waves in a rectangular channel, by a similarity transformation of time and longitudinal coordinate with a scaling factor (later referred to as κ in Teng and Wu[6,7]) which depends purely on the channel cross-sectional geometry below the unperturbed water surface. In other words, this analogous principle predicts that, under conditions of equal mean water depth and equal mean wave amplitude, the wavelength of free traveling waves in a non-rectangular channel with shape factor κ will be κ times the wavelength in a corresponding rectangular channel [whose $\kappa \equiv 1$ by definition; see (7)]. So far, this important theoretical result has not been investigated experimentally. (Waves propagating in non-rectangular channels were also studied theoretically by Shen,[8,9] and Shen and Zhong,[10] though without addressing the analogous principle.)

In Teng and Wu,[6] previous studies by Peters[5] and Peregrine[3] were extended from the physically closed case of free traveling waves in uniform channels to the more general open cases of forced production of long waves in variable channels. They showed for a long wave of mean elevation $\zeta(x,t)$ on water moving with local section-mean velocity $u(x,t)$ along a straight uniform non-rectangular channel characterized by its shape factor κ, their channel Boussinesq equations (for modeling bidirectional waves) and their channel Kortweg-de Vries equation (for unidirectional waves) are reduced to those for a wave of elevation $\zeta'(x',t')$ and section-mean velocity $u'(x',t')$ traveling in an analogous rectangular channel by the similarity transformation

$$\begin{aligned} &x = \kappa x', \quad t = \kappa t', \quad \zeta = \zeta', \quad u = u', \\ &B(x,t) = B'(x',t'), \quad p_a(x,t) = p_a'(x',t'), \end{aligned} \tag{1}$$

where the two sets of variables are properly non-dimensionalized. Here, $p_a(x,t)$ is a given pressure distribution acting on the water surface, and $B(x,t)$ is the ''blockage ratio'' of a fully or partially submerged moving object, defined as the ratio of the local cross-sectional area of the moving object to the channel cross-sectional area. From the re-

 1070-6631/97/9(11)/3368/10/$10.00

sults of similarity transformation (1), a uniform channel wave theorem was proposed by Wu (Teng and Wu[6]), which states that to a long wave of wavenumber k, period T, phase velocity c and amplitude α evolving in a κ-shaped uniform channel, there corresponds an analogous wave of wavenumber k', period T', phase velocity c' and amplitude α', evolving in an analogous rectangular channel according to

$$k' = \kappa k, \quad T' = T/\kappa, \quad c' = c, \quad \text{and} \quad \alpha' = \alpha, \tag{2}$$

in addition to having the waves satisfy the similarity relations in (1).

In the last two decades, various studies were carried out by Wu and Wu,[11,12] Akylas,[13] Ertekin, Webster and Wehausen,[14] Mei,[15] Lee, Yates and Wu,[16] Ertekin, Qian and Wehausen,[17] Teng and Wu[18,19] and others to investigate the nonlinear phenomenon of periodic production of upstream-radiating solitary waves (also called run-away solitons) by disturbances steadily moving at critical speeds in rectangular channels. Results showed that, for a rectangular channel, whether the disturbances (such as submerged moving objects) are two- or three-dimensional, the run-away solitons generated by them are invariably two-dimensional with a uniform crest across the channel. To investigate the forced run-away solitons in wide trapezoidal channels, Mathew and Akylas[20] derived a forced K–P equation by using perturbation expansion, and their numerical results showed that the wave height of forced waves in a wide trapezoidal channel can vary significantly across the channel. If these cases are extended to channels of arbitrary shape, the time period of resonant wave generation is expected to be affected by channel geometries in accordance with the similarity rules of (1) and (2), a conjecture to be verified in the present study. Another important category of time-dependent motions is the wave–wave interaction between two solitary waves during their collision, in which case the duration of encounter is shown by Wu[21,22] to be also channel-shape dependent.

In the present study we focus on examining the channel-shape effect on the *longitudinal wave profile* and on the *time period of wave generation under resonant forcing* through both theoretical analysis and experimental measurement. The original uniform channel wave theorem, similar to Peters'[5] and Peregrine's[3] analogous principle, was meant to hold for channels whose sidewalls are vertical or close to vertical at the water surface since the effect of channel sidewall slope at the waterline was neglected in the original derivation.[6] In the present study, this effect was further taken into account in our modeling of the first-order mean flow, and a set of more consistent channel Boussinesq and KdV equations were derived.

Results indicate that the channel sidewall slope at the waterline, represented by a slope factor γ (defined as the channel sidewall slope divided by the channel surface width), affects both the longitudinal and lateral wave profiles, the time period of wave generation, and the wave speed. Compared with waves in a channel with vertical sidewalls at the waterline, waves in a channel with outward fanning sidewalls at the waterline will have a longer wavelength and a longer time period of resonant wave generation, but slower wave speed. Based on these new results, the original uniform channel wave theorem has been modified. The effect of the channel sidewall slope was first studied by Peters[5] and Peregrine,[3] and the present theoretical results are an extension of their earlier work.

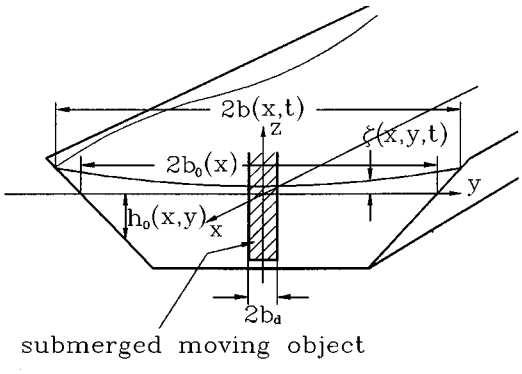

FIG. 1. A sketch of a non-rectangular channel with a coordinate set-up.

In addition to theoretical modeling, the present study is devoted to examine the validity of existing[3,5,6] and our new theories by performing experiments using two different channels. Specifically, the longitudinal wave profile of free traveling solitary waves and time period of wave generation of resonantly forced run-away solitons in a rectangular channel ($\kappa \equiv 1$, $\gamma = 0$) and a trapezoidal channel ($\kappa = 1.27$, $\gamma = 0.16$) were measured. For free traveling solitary waves, wave profiles in both the longitudinal and lateral directions were recorded for four different wave amplitudes. For resonantly forced waves, a hydrofoil was towed at critical speed in the rectangular and the trapezoidal channels to generate a series of upstream-advancing solitary waves with the time period of wave generation measured. These experimental results were then compared with the theoretical predictions based on the existing and our new wave models.

II. SECTION-MEAN LONG WAVE EQUATIONS

For long waves generated and propagated in a shallow water channel with sloping sidewalls (see Fig. 1), the section-mean continuity and momentum equations for inviscid and incompressible flows are given as

$$A_t + (A\overline{u})_x = 0, \tag{3}$$

$$(A\overline{u})_t + (A\overline{uu})_x = -A\overline{p_x}, \tag{4}$$

where $A(x,t)$ is the instantaneous cross-sectional area of the flow, u the longitudinal fluid velocity and p the pressure. The x-coordinate is set up along the channel centerline, and the overlines in the equations denote quantities averaged over the channel cross-sectional area. All variables have been non-dimensionalized according to

$$x = x^*/\lambda^*, \quad (y,z) = (y^*,z^*)/H^*, \quad t = t^* c_0^*/\lambda^*,$$

$$u = u^*/c_0^*, \quad p = p^*/\rho^* c_0^{*2}, \quad A = A^*/H^{*2},$$

where H^* is the typical unperturbed mean water depth, c_0^* ($=\sqrt{gH^*}$, with g being the gravitational acceleration) is the critical linear wave speed, ρ^* the water density, and λ^* the typical wavelength. The symbol "*" denotes dimensional

quantities. The present study is focused on Boussinesq's class of weakly nonlinear and weakly dispersive long waves where, if we define $\alpha=a^*/H^*$ and $\epsilon=H^*/\lambda^*$ with a^* being the typical wave amplitude, we have $O(\alpha)=O(\epsilon^2)$ implying that the nonlinear and dispersive effects are of equal importance for small parameters $\alpha \ll 1$ and $\epsilon \ll 1$.

The instantaneous cross-sectional area $A(x,t)$ can be written as $A(x,t)=A_0(x)-A_d(x,t)+A_\zeta(x,t)$ with A_0 being the unperturbed cross-sectional area, A_d the area reduction due to a submerged object moving below the unperturbed water surface and A_ζ the cross-sectional area due to wave elevation ζ of the free surface. The last term A_ζ can be further expressed as

$$A_\zeta=\int_{-b_0}^{b_0}\zeta dy-\int_{-b_d}^{b_d}\zeta dy+2\int_{b_0}^{b}\left[\zeta-\frac{1}{S}(y-b_0)\right]dy, \tag{5}$$

where for simplicity, the channel has been assumed to be symmetric about its centerline. (Asymmetric channels can be modeled similarly, as will be discussed in section V.) In this expression, $2b_0$ is the unperturbed channel surface width, $2b$ the instantaneous surface width, $2b_d$ the width of the moving object and $S=dy/dz$ is the channel sidewall slope (with respect to the vertical) at the waterline. For the last integral in (5), we can also write $y-b_0=Sz$, and the integrand becomes $\zeta-z$ for $y\in(b_0,b)$. If the sidewalls are vertical, then $|z|\leqslant\zeta$ (finite), and $b=b_0$, which shows that the last integral in equation (5) will vanish when $S=0$.

For shallow water long waves propagating in a channel that is not excessively wide, the dominant wave motion is in the longitudinal direction and flows in the transversal and vertical directions are secondary. Thus we can introduce the following perturbation expansions in terms of α:

$$u(x,y,z,t)=\alpha u_1(x,t)+\alpha^2 u_2(x,y,z,t)+\cdots,$$

$$\zeta(x,y,t)=\alpha\zeta_1(x,t)+\alpha^2\zeta_2(x,y,t)+\cdots,$$

$$\phi(x,y,z,t)=\alpha\phi_1(x,t)+\alpha^2\phi_2(x,y,z,t)+\cdots,$$

where ϕ is the velocity potential, scaled by $c_0^*\lambda^*$. The magnitude of the external forcing parameters A_d, b_d and p_a are all assumed to be of $O(\alpha^2)$ as weak forcings applied to the water system, and spatial variation in A_0 is assumed to be gradual, i.e., $A_{0x}=O(\alpha)$. By defining the ''width-mean'' as

$$(\tilde{\cdot})=\frac{1}{2b_0}\int_{-b_0}^{b_0}(\cdot)dy,$$

we can approximate the change in channel surface width, $b-b_0$, in terms of $\tilde{\zeta}$ and S as $b-b_0=S\tilde{\zeta}+O(\alpha^2)$. Substituting this result into (5) and keeping all terms to $O(\alpha^2)$, we have

$$A_\zeta=2b_0\tilde{\zeta}+S\tilde{\zeta}^2+O(\alpha^3). \tag{6}$$

In the original derivation,[6] the term $S\tilde{\zeta}^2$ was neglected. With this term added and following the same steps in Teng and Wu,[6,7] the extended channel Boussinesq equations can be derived as

$$(2b_0\zeta+S\zeta^2)_t+[2b_0(h_0+\zeta)u]_x=(A_d)_t,$$

$$u_t+uu_x+\zeta_x-\tfrac{1}{3}\kappa^2h_0^2u_{xxt}=-(p_a)_x,$$

where the overlines and tildes for $\overline{u}$, $\tilde{\zeta}$, $\tilde{h}_0$ (for h_0, see Fig. 1), $\tilde{p}_a$ have been omitted for simplicity, and x and t have been rescaled by H^* and H^*/c_0^*, respectively. In these equations, two factors related to channel geometry affect the generation and propagation of long waves. One factor is the channel shape factor, κ, which depends purely on the unperturbed channel cross-sectional geometry, and is given by

$$\kappa^2=\frac{3}{h_0}(\tilde{\Psi}-\overline{\Psi}), \tag{7}$$

where

$$\tilde{\Psi}=\frac{1}{2b_0}\int_{-b_0}^{b_0}\Psi(y,0;x)dy,$$

$$\overline{\Psi}=\frac{1}{A_0}\int\int_{A_0}\Psi(y,z;x)dydz, \tag{8}$$

with Ψ satisfying the following equation and boundary conditions in the cross-flow plane (Teng and Wu[6,7]):

$$\Psi_{yy}+\Psi_{zz}=1, \tag{9}$$

$$\Psi_z|_{z=0}=h_0 \quad \text{(at the free surface)}, \tag{10}$$

$$\Psi_n=0 \quad \text{(at channel walls below the unperturbed water surface)}, \tag{11}$$

where $\vec{n}$ is the unit normal vector at the channel walls in the cross-flow plane. The right-hand-side of equation (7) is always positive and therefore κ is always real (for a proof, see Appendix A). By definition (7), $\kappa\equiv 1$ for rectangular channels.[6] For non-rectangular channels, if the channel shape is such that the width increases (or decreases) from the channel bottom to the surface, then the κ value will be greater (or smaller) than one. (Values of κ for several specific channel geometries were given in Teng and Wu.[6,7])

The other geometric factor is S, the channel sidewall slope at the waterline. Quantitative effects of these two parameters (i.e., κ and S) will be discussed in detail in the next section.

For unidirectional motion, the channel KdV equation can be derived from the Boussinesq equations to obtain

$$\pm\frac{1}{\sqrt{h_0}}\zeta_t+\zeta_x+\left(\frac{3}{2h_0}-\frac{S}{2b_0}\right)\zeta\zeta_x+\frac{1}{6}\kappa^2h_0^2\zeta_{xxx}$$

$$+\tfrac{1}{4}[\ln(h_0b_0^2)]_x\zeta=-\tfrac{1}{2}(B+p_a)_x,$$

where the forcing function B is given by $B=A_d^*/A_0^*=A_d/2b_0$, which represents the cross-sectional blockage-ratio of a submerged moving object. The $+$ (or $-$) sign in the KdV equation applies to right-going (or left-going) waves.

After the mean wave elevation $\tilde{\zeta}$ is solved by using either the Boussinesq or the KdV equations, the local variation of wave elevation across the channel can be solved by using the unsteady Bernoulli equation to get

$$\zeta(x,y,t)=-\phi_t-\tfrac{1}{2}\phi_x^2+O(\alpha^3)=\tilde{\zeta}(x,t)-(\Psi|_{z=0}-\tilde{\Psi})\tilde{\zeta}_{xx}. \tag{12}$$

Based on this theory, the ''mean wave position,'' y_m, defined by $\zeta(x,y_m,t)=\tilde{\zeta}(x,t)$, can be derived from (12) as the root of the equation

$$\Psi(y_m,0;x)-\frac{1}{2b_0}\int_{-b_0}^{b_0}\Psi(y,0;x)dy=0. \tag{13}$$

In deriving these results, we have used the first-order approximations $\zeta=\pm c_o u$ and $\partial_t=\mp c_o\partial_x$, with the upper (or lower) sign for right-going (or left-going) waves, in modifying the second-order terms.

III. LONG WAVES IN UNIFORM CHANNELS

For waves in uniform channels ($h_0=H=1$, $b_0=$constant), the channel Boussinesq equations are reduced to

$$(\zeta+\gamma\zeta^2)_t+[(1+\zeta)u]_x=B_t, \tag{14}$$

$$u_t+uu_x+\zeta_x-\tfrac{1}{3}\kappa^2u_{xxt}=-(p_a)_x, \tag{15}$$

and for right-going waves, the KdV equation becomes

$$\zeta_t+\zeta_x+(\tfrac{3}{2}-\gamma)\zeta\zeta_x+\tfrac{1}{6}\kappa^2\zeta_{xxx}=-\tfrac{1}{2}(B+p_a)_x, \tag{16}$$

where the waterline slope factor $\gamma=S/2b_0$. If the channel sidewall at the waterline is vertical ($\gamma=0$) or close to vertical [$\gamma=O(\alpha)$], then by the similarity transformation (1), the equations of both the Boussinesq and the KdV models for describing long waves in a non-rectangular channel will be reduced to that for waves in a rectangular channel according to the uniform channel wave theorem.

For channels whose sidewalls are not vertical at the waterline [say, $\gamma=O(1)$], similarity transformations have not been found for the Boussinesq model. For the KdV equation, if we follow Peregrine's[3] approach and introduce the following change of variables:

$$\hat{\zeta}=\beta\zeta,\quad \hat{B}=\beta B,\quad \hat{p}_a=\beta p_a;\quad \text{with}\ \ \beta=1-\tfrac{2}{3}\gamma, \tag{17}$$

the KdV equation will become

$$\hat{\zeta}_t+\hat{\zeta}_x+\tfrac{3}{2}\hat{\zeta}\hat{\zeta}_x+\tfrac{1}{6}\kappa^2\hat{\zeta}_{xxx}=-\tfrac{1}{2}(\hat{B}+\hat{p}_a)_x,$$

which can be further reduced to the equation for waves in a rectangular channel by similarity transformation (1). Hence, for unidirectional wave motion in a uniform channel with sloping sidewalls at the waterline, the original uniform channel wave theorem can be modified according to (17) and (1), based on the KdV model.

For a free traveling solitary wave of permanent shape, its solution based on the KdV equation is readily obtained as

$$\zeta=\alpha\,\mathrm{sech}^2\sqrt{\frac{3\beta\alpha}{4\kappa^2}}(x-ct),\quad \text{with}\ \ c=1+\beta\frac{\alpha}{2}, \tag{18}$$

which shows that the wave profile depends on both the unperturbed cross-sectional geometry (characterized by κ) and the channel sidewall slope factor γ at the waterline, whereas the dimensionless wave speed c is affected only by the slope factor γ. Compared with waves in a channel with vertical sidewalls at the waterline, waves in a channel with outward fanning ($\gamma>0$) sidewalls at the waterline will have a longer wavelength but a slower wave speed. The effect of S is more significant for narrow channels than for wide channels because $\gamma(=S/2b_0)$ increases with decreasing b_0 for a fixed S. Based on the KdV equation (16), if $\gamma\geqslant 1.5$, positive solitary waves can no longer exist.

The solitary wave solution of the Boussinesq equations (14)–(15) was solved recently in Teng,[23] and the results are briefly listed here. First, the velocity $u=cv$ is solved through

$$x-ct=\pm\int_{v_c}^{v}\frac{dv}{[G(v;c)]^{1/2}},$$

where

$$\begin{aligned}G(v;c)=\frac{3}{\kappa^2\gamma c^2}\Bigg[&v-\frac{1}{2}(1-2\gamma c^2)v^2-\frac{1}{3}\gamma c^2v^3\\&-\frac{1}{2}(v-1+2\gamma)\sqrt{v^2-2(1-2\gamma)v+1}\\&-2\gamma(1-\gamma)\ln\frac{1}{2\gamma}(v-1+2\gamma\\&+\sqrt{v^2-2(1-2\gamma)v+1})+\gamma-\frac{1}{2}\Bigg]\end{aligned}$$

and v_c is the maximum value of v given by

$$v_c=(1+\gamma\alpha)\frac{\alpha}{1+\alpha}.$$

After v is solved, the wave elevation ζ can be obtained through

$$\zeta=\frac{1}{2\gamma}[-(1-v)+\sqrt{(1-v)^2+4\gamma v}],$$

and the wave speed c is given by an explicit analytical solution as

$$\begin{aligned}c^2=\frac{1}{\gamma v_c^2(1-\frac{1}{3}v_c)}\Bigg[&-v_c+\frac{1}{2}v_c^2+\frac{1}{2}(v_c-1+2\gamma)\\&\times\sqrt{v_c^2-2(1-2\gamma)v_c+1}+2\gamma(1-\gamma)\ln\frac{1}{2\gamma}(v_c-1\\&+2\gamma+\sqrt{v_c^2-2(1-2\gamma)v_c+1})-\gamma+\frac{1}{2}\Bigg].\end{aligned}$$

Again, it is noted that the wave speed c depends on γ but is independent of κ.

In Fig. 2(a), solitary wave profiles of amplitude $\alpha=0.34$ in a rectangular channel ($\kappa\equiv 1,\gamma=0$), a trapezoidal channel ($\kappa=1.27$) with outward fanning sidewalls inclined at 45° to the horizontal ($\gamma=0.16$), and a trapezoidal channel ($\kappa=1.27$) similar to the previous one but with the sidewalls becoming vertical at the waterline ($\gamma=0$) are compared based on the Boussinesq solution. The specific cross-sectional geometry of the trapezoidal channel is shown in Fig. 3(c). From Fig. 2(a), it can be seen that the longitudinal wave profile is affected by both the shape factor κ and the slope factor γ, and the larger the κ and γ values, the longer the wave. Figure 2(b) shows the comparison between the wave profiles based on the KdV and the Boussinesq solu-

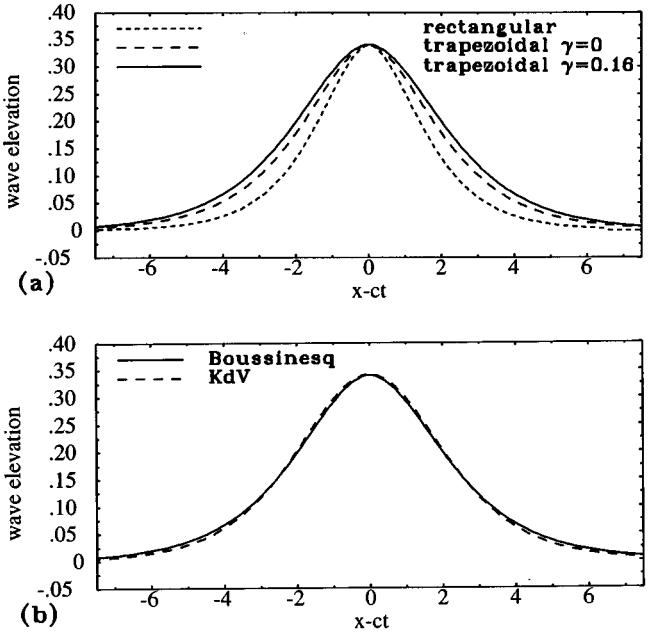

FIG. 2. Theoretical solitary wave profiles in channels of different geometry; (a) solitary wave profile of amplitude $\alpha=0.34$ based on the Boussinesq solution in a rectangular channel with $\kappa=1$ and $\gamma=0$ (short dashed line); in a trapezoidal channel with $\kappa=1.27$ and $\gamma=0$ (long dashed line); and in a trapezoidal channel with $\kappa=1.27$ and $\gamma=0.16$ (solid line). (b) Comparison of the wave profile between the KdV (dashed line) and the Boussinesq (solid line) solutions for $\alpha=0.34$ with $\kappa=1.27$ and $\gamma=0.16$.

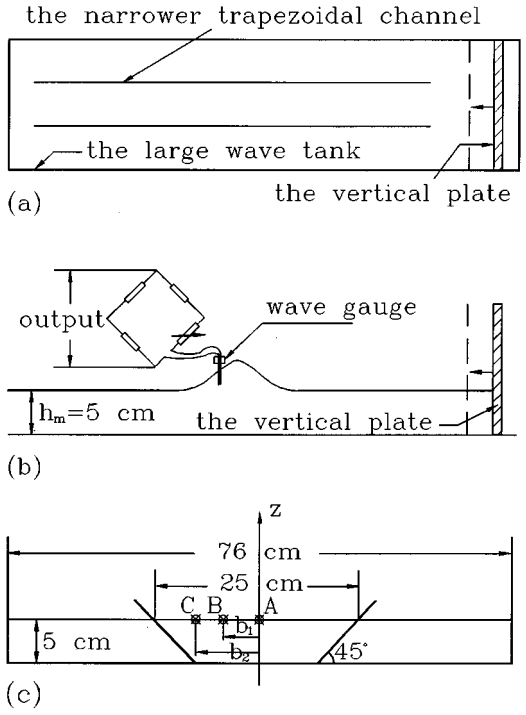

FIG. 3. Experimental set-up to study free traveling solitary waves in a trapezoidal channel; (a) top view; (b) side view; (c) end view. Gauge A: at centerline; gauge B: $b_1=4.4$ cm; gauge C: $b_2=7.6$ cm. (This figure is not drawn to scale.)

tions for $\alpha=0.34$, $\kappa = 1.27$ and $\gamma=0.16$. The result shows that the difference between the two is very small.

Detailed discussions on the wave speed and the critical value of γ for solitary waves to exist based on the Boussinesq and KdV solutions can be found in Teng.[23]

IV. EXPERIMENTAL SET-UP AND RESULTS

The experiments were conducted in a wave tank 7.5 m long, 0.76 m wide and 0.6 m high. A narrower uniform channel was constructed inside the wave tank by using Plexiglas plates, as shown in Fig. 3(a). The width and sidewall inclination angle of the narrower channel were adjustable, so that different rectangular and trapezoidal channels could be constructed. The wave tank was equipped with a towing carriage that was controlled by a motor with adjustable speed. Wave elevations were measured by resistance-type wave gauges which were calibrated before and after each run in the experiment.

We first tested the accuracy of our instruments by measuring the longitudinal wave profile of free traveling solitary waves in the main rectangular wave tank, since solitary waves in rectangular channels have been well investigated and are usually used as a standard wave profile to test the wave measurement system. In our test, a solitary wave was generated by pushing a vertical plate for a short distance (usually around 5 to 10 cm) at one end of the main wave tank, as shown in Figs. 3(a) and 3(b) without the narrower trapezoidal channel. Four wave gauges were placed at different locations sufficiently far downstream where the solitary wave was fully developed. For each run, the four gauges recorded almost the same amplitude and wave profile indicating that, for a solitary wave in a rectangular channel, the wave crest is uniform over its span, and the wave propagates permanent in shape and speed except for a small damping. Figure 4 shows the comparison between the measured (solid line) and the theoretical (KdV, dashed line) solitary wave profiles for wave amplitudes of $\alpha=0.25$ and 0.43 in the rectangular channel. Note that the measurements were made by fixed wave gauges which recorded a time series of wave elevation at a fixed location instead of the wave profile at a frozen instant. However, the duality in space and time is clear, as for a solitary wave, $\zeta=\zeta(x-x_0-c(t-t_0))$, the time series at location x_0, $\zeta(-c(t-t_0))$, is related to the spatial distribution at time t_0, $\zeta(x-x_0)$, with c being a constant. For convenience of comparison, the origin of the time records in Fig. 4 has been shifted in order to set the wave peak at $T=0$ of the new shifted time T. Results from Fig. 4 show that the measured wave profiles agree very well with the theoretical profiles.

A. Channel-shape effects on free traveling long waves

To investigate the effect of channel geometry on shallow water long waves, a trapezoidal channel was constructed inside the main wave tank as shown in Fig. 3. The water depth was 5 cm at the channel centerline and the channel width was 25 cm at the unperturbed water surface. The sidewalls were inclined at $\theta=45°$ to the horizontal. For this set-up, the mean water depth was $h_0=4$ cm and the shape factor κ was

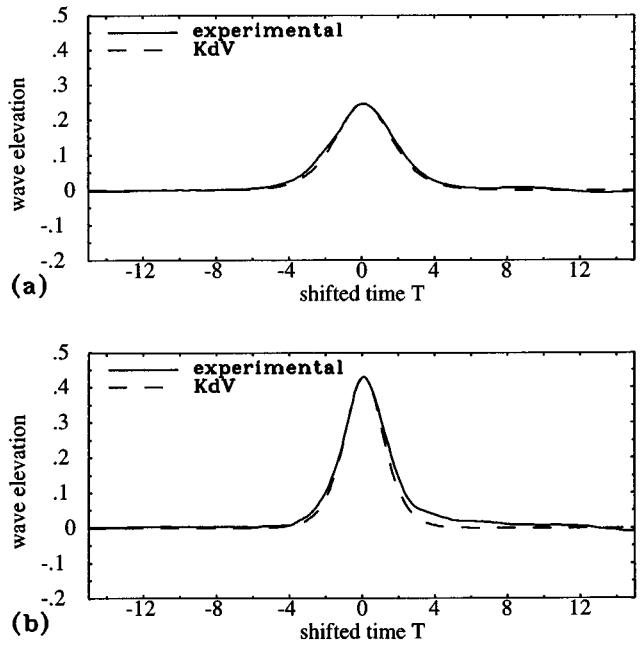

FIG. 4. Comparison between measured (solid line) and theoretical (KdV, dashed line) solitary wave profiles in the main rectangular channel; (a) $\alpha = 0.25$; (b) $\alpha = 0.43$.

calculated to be $\kappa = 1.27$ by solving (9)–(11) numerically using the Gauss–Seidel iterative scheme. The slope factor $\gamma = 0.16$.

To capture the longitudinal wave profile and also to monitor the transverse wave variation, several wave gauges were placed over a fixed cross section inside the trapezoidal channel where the solitary wave was fully developed, as sketched in Figs. 3(a)–3(c). Among these gauges, wave gauge C was held at $y_m = 7.6$ cm from the centerline and used to measure the ''mean wave elevation,'' as consistent with the theory. This particular position at $y_m = 7.6$ cm was determined by solving (13) for the specific trapezoidal geometry in the present case.

For comparison purposes, free solitary waves were also measured in the main rectangular wave tank of width 0.76 m and water depth 4.0 cm which was set to equal the mean water depth in the trapezoidal channel. Solitary waves of four different amplitudes, $\alpha = 0.12$, 0.25, 0.34 and 0.43, were recorded and compared between the rectangular and trapezoidal channels. For each amplitude in each channel, three runs were repeated, and the results from different runs were found to be very consistent.

Comparative results from the two channels (Fig. 5) show that, under conditions of equal mean water depth and equal mean wave amplitude, a solitary wave in the trapezoidal channel appears to be significantly longer than that in the rectangular channel, just as predicted by existing theories.[3,5,6] We notice that the solitary waves in the trapezoidal channel do not appear as ''clean'' as those in the rectangular channel, especially near the tail. This is caused by the unavoidable three-dimensional wave features in a non-rectangular channel, as also observed and explained by Peregrine.[4]

In order to examine the validity of the similarity trans-

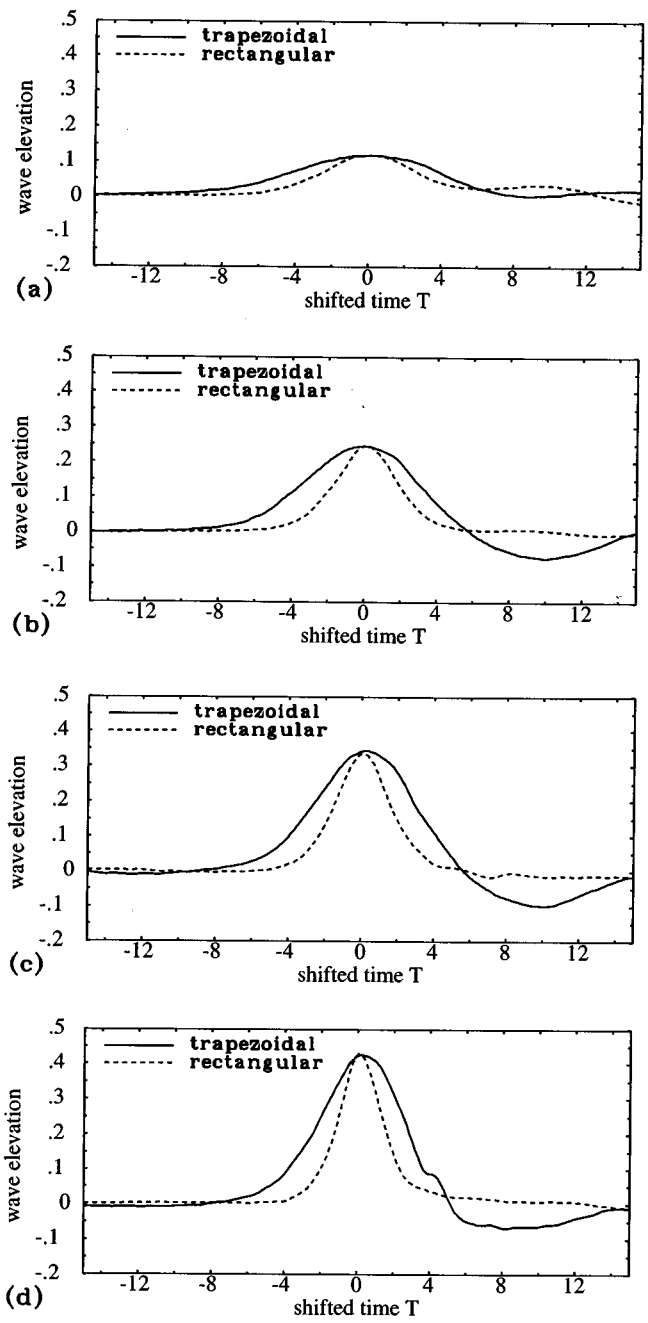

FIG. 5. A comparison of measured solitary wave profiles in the trapezoidal and rectangular channels; solid line: waves in the trapezoidal channel; dashed line: waves in the rectangular channel; (a) $\alpha = 0.12$; (b) $\alpha = 0.25$; (c) $\alpha = 0.34$; (d) $\alpha = 0.43$. The mean water depths in the two channels are the same.

formation (1), (2) and (17), the measured wavelength ratio λ_t/λ_r (here λ_t and λ_r represent wavelengths in the trapezoidal and rectangular channels, respectively) was determined and compared with the predicted ratio, which equals $\kappa(1 + \alpha/2)/\sqrt{\beta}(1+\beta(\alpha/2))$ based on the KdV solution (18). In this study, the measured λ_t/λ_r ratio was determined by rescaling the T variable with a constant C for the wave profile in the trapezoidal channel, and the resulting profile $\zeta(CT)$ was plotted against the wave profile in the rectangular channel in the same graph. The constant C was then adjusted for

TABLE I. Comparison between the measured and predicted ratio of λ_t/λ_r.

α	Measured λ_t/λ_r	Predicted λ_t/λ_r	Relative difference
0.12	1.45	1.352	7%
0.25	1.65	1.360	21%
0.34	1.68	1.365	23%
0.43	1.82	1.370	33%

the best match of the wave profiles in the two channels. The final value of this constant is taken as the measured wavelength ratio. The detailed results are listed in Table I.

From these results, we can see that for a small wave amplitude (e.g., $\alpha=0.12$), the existing theories give good prediction for the channel-shape effect as measured in the experiment. This is consistent with the theoretical validity criteria of $\alpha \ll 1$ based on the perturbation theory. For large-amplitude waves, there are some quantitative differences between the experiment and the theory, and the discrepancy increases as wave amplitude increases. Possible cause for this discrepancy for large-amplitude waves will be discussed in section V.

B. Channel-shape effects on resonantly forced long waves

Experiments to examine the channel-shape effect on forced long waves were carried out where a submerged hydrofoil was towed at critical speed in a rectangular and a trapezoidal channel ($\kappa=1.27$, $\gamma=0.16$) constructed inside the main wave tank separately. The experimental set-up and the dimensions of the two channels along with the hydrofoil are shown in Figs. 6(a) and 6(b). The discretized width function $2b_d$ of the hydrofoil is given in Appendix B. For both channels, the mean water depth was 4.0 cm and the blockage-ratio B was $0.752b_d$, where b_d is the dimensionless half-thickness of the hydrofoil. Also, in both cases, the hydrofoil was towed to move with the same dimensionless critical speed of $Fr=U/c_0=0.99$.

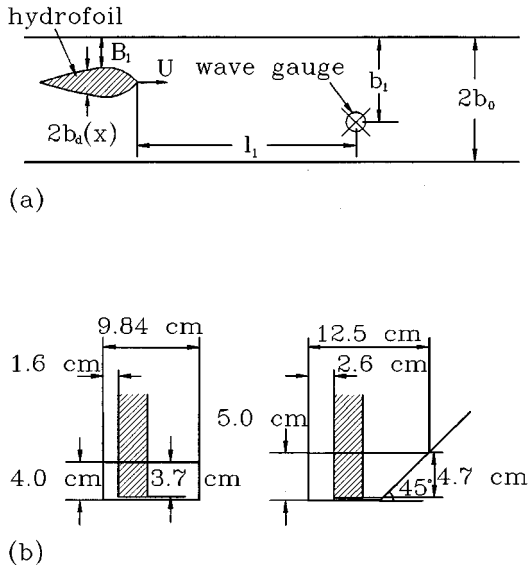

FIG. 6. The experimental set-up for resonantly forced long waves by a hydrofoil towed at critical speed in a trapezoidal and a rectangular channel; (a) top view; (b) end view; on the left: rectangular channel; on the right: trapezoidal channel. B_1: distance from one sidewall to the widest point of the hydrofoil. For the trapezoidal channel: $2b_0=12.5$ cm, $B_1=2.6$ cm, $l_1=38.8$ cm and $b_1=7.6$ cm; for the rectangular channel: $2b_0=9.84$ cm, $B_1=1.6$ cm, $l_1=38.8$ cm and $b_1=4.86$ cm.

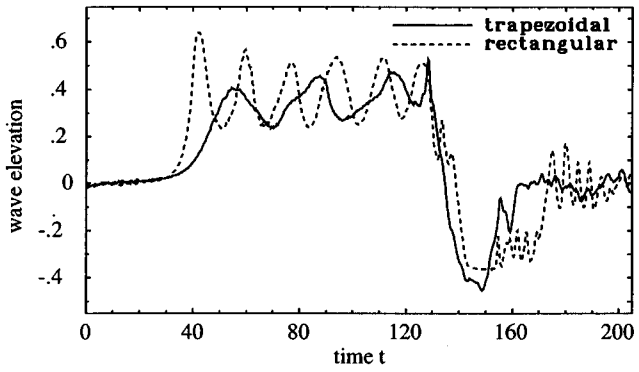

FIG. 7. Comparison of measured experimental results of the resonantly forced long waves in the trapezoidal channel (solid line) and the rectangular channel (dashed line).

In the experiment, wave elevation was measured by a wave gauge fastened to the towing carriage 38.8 cm in front of the hydrofoil. For the rectangular channel, this wave gauge was placed 4.86 cm from one of the sidewalls, while in the trapezoidal channel it was fixed at 7.6 cm away from the vertical wall. In each experiment, the hydrofoil was towed from rest and accelerated to the critical speed in less than 0.5 s and then continually moved at a constant critical speed over a distance of $L=5.1$ m before being brought to a stop. In dimensionless form, the total time that the hydrofoil traveled is 128.3, during which the hydrofoil traveled a distance of about 128 mean water depths. For waves generated in the rectangular channel, the experiment was repeated six times, and in the trapezoidal channel, three runs were conducted.

Typical results of long waves resonantly produced in the two channels are shown and compared in Fig. 7, with the solid line representing the waves generated in the trapezoidal channel, and the dashed line showing the waves in the rectangular channel. Under conditions of the mean water depth, disturbance speed and blockage-ratio all kept equal for both channels, results show that during the same time period, there were six run-away solitons generated in the rectangular channel whereas only slightly more than three were produced in the trapezoidal channel. Obviously, the channel cross-sectional geometry has a significant effect on wavelength and time period of wave generation as predicted by the theory.

To verify the theory quantitatively, we need to compare the measured time period of wave generation, T_s, with that predicted by the theory. Here T_s is defined as the time period between two consecutive wave peaks in the time record of wave elevation of the run-away solitons generated in front of the disturbance. The final measured time period of wave generation T_s in each channel was represented by the average T_s

TABLE II. Comparison between the measured and predicted T_s.

	Measured	Predicted	Relative difference
T_{st}	29.1	33.2	12%
T_{sr}	17.5	19.8	12%

calculated from all the waves measured over all the repeated runs. For the rectangular channel, the recorded average T_s is 17.5, and for the trapezoidal channel, $T_s=29.1$. In the present case, the uniform channel wave theorem cannot be directly applied to give the theoretical ratio of T_{st}/T_{sr} (here T_{st} and T_{sr} stand for time period of wave generation in the trapezoidal and rectangular channels, respectively) since, for the convenience of experiment, we used the same hydrofoil in both channels instead of using two separate hydrofoils with their longitudinal length and lateral thickness properly scaled according to (17) and (1). To calculate the theoretical T_s, we carried out numerical simulations of these experiments by solving the original KdV equation (16). In our computations, the viscous effect in real flows is considered by adding a boundary layer displacement thickness 2δ to the hydrofoil thickness $2b_d$, one δ for each side of the hydrofoil surface. For the present case, the Reynolds number is calculated to be $Re=Ul/\nu=Frcl/\nu=0.99\times\sqrt{9.81\times0.04}\times0.092/10^{-6}=5.7\times10^4$, where U is the hydrofoil speed and l is the chord length of the hydrofoil. As an approximation, the Blasius solution for laminar boundary layer over a flat plate was used to estimate the boundary layer thickness $2\delta(x)$ for the hydrofoil:

$$2\delta(x)=2\times4.92\times\sqrt{\frac{\nu}{h_0U}(-x)}=0.06216\sqrt{-x},$$

$$\text{for } -2.3\leqslant x\leqslant 0,$$

where δ and x are in dimensionless form. Quantitative comparison between experimental and theoretical values for time period of wave generation T_s is given in Table II.

From the results presented in Table II, it can be seen that the theory gives a good prediction for the time period of wave generation under resonant forcing, and this confirms the theoretical prediction on the channel-shape effect.

V. DISCUSSIONS

In our experiments, instrumental error mainly came from errors in the tape measures and the stop watch that were used. Surface tension effect and electronic noises in the wave transducers also contributed to this error. With all the factors considered, the *maximum* accumulative instrumental error is estimated as 7% for measurement of free traveling waves and 14% for that of the forced waves. The magnitude of these errors is comparable with that in other previous studies using similar instruments to measure shallow water waves. In order to rule out accidental errors, each measurement was repeated for several times. Results from repeated runs are very consistent with one another. For example, for measurement of the forced waves, the sample standard deviation is calculated to be 0.016 for the wave amplitude and 0.7 for the time period of wave generation, averaged over the results from both channels.

TABLE III. Estimate for the higher-order error in channel width approximation.

$\overline{\alpha}$	Instantaneous b	Unperturbed b_0	Relative difference
0.12	3.262	3.125	4%
0.25	3.438	3.125	10%
0.34	3.588	3.125	15%
0.43	3.788	3.125	21%

The quantitative differences between the experimental results and the theoretical predictions for large-amplitude waves in the trapezoidal channel may be partially caused by the experimental error and partially by the higher-order error related to the cross-flow solution (8)–(11) in the existing theories which approximate the instantaneous channel surface width $2b$ with the unperturbed width $2b_0$. This approximation is proper for modeling small-amplitude waves based on the perturbation theory, since the cross-flow solution is considered as being of higher order compared with the mean flow, and for consistency, all higher-order terms should be neglected in the cross-flow solution. However, as wave amplitude increases, the change in channel surface width also increases due to wave run-up onto the sloping banks, and the terms neglected may no longer be of higher order. To give a rough estimate for this error, equation (12) was applied to solve for the transverse profile of solitary waves of mean amplitude $\alpha=0.12$, 0.25, 0.34 and 0.43 in the trapezoidal channel shown in Fig. 3(c). By using linear extrapolation, the wave profile was extended along the wave crest to intersect with the sloping sidewalls to determine the predicted instantaneous channel surface width. These results are presented in Table III and in Fig. 8.

Results from Table III and Fig. 8 show that, as wave amplitude increases, the error in approximating the instantaneous width with the unperturbed width also increases, and the error can be as large as 21% for $\alpha=0.43$. In Peregrine's[4] experimental study to investigate the lateral wave profile of

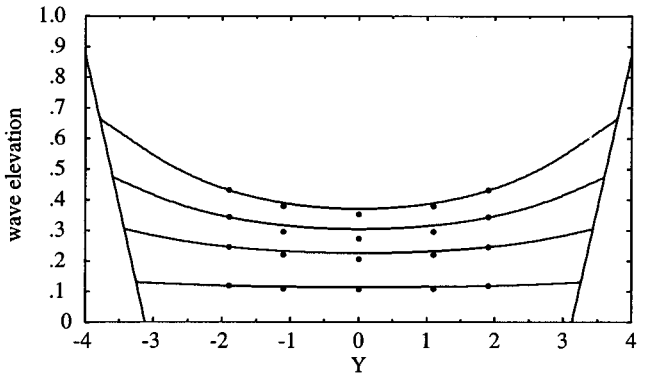

FIG. 8. Variation of solitary wave amplitude across the trapezoidal channel. Curved solid lines: theoretical wave profiles of mean amplitude $\alpha=0.12$, 0.25, 0.34 and 0.43; solid dots: experimental data; two straight solid lines: the inclined channel sidewalls.

solitary waves in similar trapezoidal channels, the actual instantaneous channel width was recorded by taking end-view photographs. His results showed that, for $\alpha \approx 0.2$, the difference between the actual width and the approximated width was about 11%, which is consistent with our present estimate.

In the present experiment, the lateral wave variation in the trapezoidal channel was measured by wave gauges at several fixed locations within the unperturbed channel width $2b_0$. These experimental results are shown with solid dots in Fig. 8. We can see that, for small-amplitude waves, the measured wave variation across the channel agrees very well with the theoretical predictions, while for large-amplitude waves, there are some small but discernible differences between the theory and the experiment.

These results indicate that the accuracy of the existing theories for describing large-amplitude waves in non-rectangular channels may be improved if varying surface width can be properly considered in the cross-flow solution. This requires the cross-flow solution to be solved based on an equation system coupled with the first-order Boussinesq or KdV equations since in this case, the shape factor κ would depend on wave elevation and the instantaneous channel surface width. In reality, wave run-up onto sloping sidewalls is a complex problem affected by both viscous and surface tension effects and may have complex wave features such as wave breaking even when the mean wave amplitude is as small as $\alpha = 0.3$, as observed in both Peregrine's[3] and our present studies. It is of interest to improve the inviscid theory to accurately predict the wave run-up, and further research is needed to better handle this complex ''edge effect.''

The existing and our new theories also provide solutions for wave speed, and they predict that the dimensionless wave speed is dependent on the channel sidewall slope at the waterline. This issue was not investigated in the present experiments, because the difference in wave speed between two different channels can be relatively small. For example, the relative difference between wave speeds in a rectangular channel and a trapezoidal channel with $\gamma = 0.16$ for $\alpha = 0.5$ is only about 2%, and our available experimental instruments do not have a sufficiently high accuracy to investigate the effect of γ on wave speed.

Another issue to be discussed is the assumption that the channels are symmetric about their centerlines. This assumption does not limit the application of our theory to channels of general geometry, since the equations presented here can be readily modified to study waves in asymmetric channels by following the same derivation steps, provided the channels remain straight. For example, if a channel has two different slopes, S_1 and S_2, for its sidewalls at the waterline, then A_ζ in (6) will be modified to give $A_\zeta = W_0 \tilde{\zeta} + \frac{1}{2}(S_1 + S_2)\tilde{\zeta}^2 + O(\alpha^3)$ with W_0 being the unperturbed channel surface width (replacing the original symbol $2b_0$). In the Boussinesq and KdV equations, S and γ will be replaced by $(S_1 + S_2)/2$ and $(\gamma_1 + \gamma_2)/2$ correspondingly. All the other formulations should remain intact.

VI. SUMMARY AND CONCLUSIONS

New Boussinesq and KdV equations are derived in this study to model long waves in shallow water channels of arbitrary shape. The main objective is to examine the channel-shape effect on long wave generation and propagation by joint theoretical and experimental studies. Our theoretical results show that, for long waves generated and propagated in a shallow water channel, the wavelength and time period of wave generation were affected by both the submerged channel cross-sectional geometry and the channel sidewall slope at the waterline. These effects of channel geometry are quantified by similarity transformations (1) and (17) based on two geometric parameters: the shape factor κ and the slope factor γ. It is shown that the wavelength and time period of resonant wave generation in a channel with larger values of κ and γ will be longer than that in a channel with smaller κ and γ.

A series of experiments were carried out to verify the existing theories. Specifically, longitudinal wave profiles of free traveling solitary waves and the time periods of wave generation of resonantly forced long waves by a towed hydrofoil were measured in a rectangular channel ($\kappa \equiv 1$, $\gamma = 0$) and a trapezoidal channel ($\kappa = 1.27$, $\gamma = 0.16$). The experimental results show that, under the condition of equal mean water depth and equal mean wave amplitude, free traveling solitary waves in the trapezoidal channel were significantly longer than that in the rectangular channel. We also observed that, under conditions of equal mean water depth and resonant forcing by submerged moving objects with equal blockage-ratio, the time period of resonant wave generation in the trapezoidal channel is longer than that in the rectangular channel by a factor as predicted. Quantitatively, the theory gives a good prediction for the time period of resonant wave generation and for the longitudinal and lateral wave profiles of free traveling solitary waves of small amplitude. These experimental results therefore verify the existing[3,5] (without forcing) and our new (with forcing) wave models derived from the Euler equations by using perturbation expansions.

There were some quantitative differences observed between the experiment and the theory for large-amplitude waves in the trapezoidal channel. One possible cause for this difference is the theoretical approximation of the instantaneous channel surface width with the unperturbed surface width in the secondary cross-flow solution, for which further improvement of the theory was suggested. More experiments may also be carried out in a future study to test out more channel geometries and to verify the effects of κ and γ separately by testing non-rectangular channels with various sidewall slopes at the waterline.

The results of the present and some related previous studies have useful applications to open channel flows and to coastal processes involving both free traveling and forced surface- and internal long waves, especially in regions where topographical and oblique boundaries are present and play an important role in wave generation and evolution as well as in mitigating ocean wave hazards in coastal regions.

ACKNOWLEDGMENTS

This work was partly sponsored by the Hawaiian Sea Grant through NOAA Grant No. NA89AA-D-SG063 and by the National Science Foundation Grant No. CMS-9503620. The authors are grateful to the reviewers for their helpful comments and suggestions.

APPENDIX A: PROOF OF κ BEING ALWAYS REAL

In this appendix, a proof is presented to show that the right-hand side of equation (7) in defining κ^2 is always positive.

For the cross-flow domain below the unperturbed water surface with area A_0 and boundary ∂A_0, we have

$$\begin{aligned}\int\int_{A_0}(\nabla\Psi)^2 dA &= \int\int_{A_0}[\nabla\cdot(\Psi\nabla\Psi)-\Psi\nabla^2\Psi]dA\\ &= \int_{\partial A_0}\Psi\Psi_n dl-\int\int_{A_0}\Psi dA\\ &= h_0\int_{-b_0}^{b_0}\Psi dy - A_0\overline{\Psi}\\ &= 2b_0h_0\widetilde{\Psi}-A_0\overline{\Psi}\\ &= A_0(\widetilde{\Psi}-\overline{\Psi}).\end{aligned}$$

Therefore, $\widetilde{\Psi}-\overline{\Psi}\geqslant 0$ and the equal sign holds only if $\Psi \equiv$constant in A_0, which is precluded by the differential equation $\nabla^2\Psi=1$. Thus we prove that $\widetilde{\Psi}-\Psi>0$ so long as the unperturbed channel surface width $2b_0$ is of finite measure.

APPENDIX B: DATA FOR HYDROFOIL THICKNESS $2b_d(x)$

The discrete data for the thickness function $2b_d(x)$ of the hydrofoil used in our experiments and numerical simulations are given as $[(-x, 2b_d)]$: (0, 0), (0.4, 1.23), (0.8, 1.81), (1.2, 2.30), (1.6, 2.60), (2.0, 2.81), (2.4, 2.94), (2.8, 3.01), (3.2, 2.97), (3.6, 2.91), (4.0, 2.80), (4.4, 2.67), (4.8, 2.50), (5.2, 2.30), (5.6, 2.10), (6.0, 1.94), (6.4, 1.73), (6.8, 1.53), (7.2, 1.37), (7.6, 1.15), (8.0, 0.96), (8.4, 0.68), (8.8, 0.44), (9.2, 0.00). The unit for both x and $2b_d$ is centimeters, and $x=0$ here is defined at the front of the hydrofoil.

[1] S. Russell, ''On waves,'' Report of the Committee on Waves, the British Association at Bristol, 7th report, 1837, Vol. VI, p. 417.
[2] J. A. Sandover and C. Taylor, ''Cnoidal waves and bores,'' Houille Blanche **17**, 443 (1962).
[3] D. H. Peregrine, ''Long waves in a uniform channel of arbitrary cross section,'' J. Fluid Mech. **32**, 353 (1968).
[4] D. H. Peregrine, ''Solitary waves in trapezoidal channels,'' J. Fluid Mech. **35**, 1 (1969).
[5] A. S. Peters, ''Rotational and irrotational solitary waves in a channel with arbitrary cross-section,'' Commun. Pure Appl. Math. **19**, 445 (1966).
[6] M. H. Teng and T. Y. Wu, ''Nonlinear water waves in channels of arbitrary shape,'' J. Fluid Mech. **242**, 211 (1992).
[7] M. H. Teng and T. Y. Wu, ''Evolution of long water waves in variable channels,'' J. Fluid Mech. **266**, 303 (1994).
[8] M. C. Shen, ''Long waves in a stratified fluid over a channel of arbitrary cross section,'' Phys. Fluids **11**, 1853 (1968).
[9] M. C. Shen, ''Asymptotic theory of unsteady three-dimensional waves in a channel of arbitrary cross section,'' SIAM (Soc. Ind. Appl. Math.) J. Appl. Math. **17**, 260 (1969).
[10] M. C. Shen and X. G. Zhong, ''Derivation of K-dV equations for water waves in a channel with variable cross section,'' J. Méc. **20**, 789 (1981).
[11] D. M. Wu and T. Y. Wu, ''Three-dimensional nonlinear long waves due to moving surface pressure,'' *Proceedings of the 14th Symposium on Naval Hydrodynamics* (National Academy Press, 1982), p. 103.
[12] D. M. Wu and T. Y. Wu, ''Precursor solitons generated by three-dimensional disturbances moving in a channel,'' *Nonlinear Water Waves*, IUTAM Symposium, Tokyo, Japan, edited by K. Horikawa and H. Maruo (Springer, Berlin, 1987), p. 69.
[13] T. R. Akylas, ''On the excitation of long nonlinear water waves by a moving pressure distribution,'' J. Fluid Mech. **141**, 455 (1984).
[14] R. C. Ertekin, W. C. Webster, and J. V. Wehausen, ''Waves caused by a moving disturbance in a shallow channel of finite width,'' J. Fluid Mech. **169**, 275 (1986).
[15] C. C. Mei, ''Radiation of solitons by slender bodies advancing in a shallow channel,'' J. Fluid Mech. **162**, 53 (1986).
[16] S. J. Lee, G. T. Yates, and T. Y. Wu, ''Experiments and analyses of upstream-advancing solitary waves generated by moving disturbances,'' J. Fluid Mech. **199**, 569 (1989).
[17] R. C. Ertekin, Z. Qian, and J.V. Wehausen, ''Upstream solitons and wave resistance,'' *Engineering Science, Fluid Dynamics* (World Scientific, Singapore, 1990), p. 29.
[18] M. H. Teng and T. Y. Wu, ''Generation and propagation of nonlinear water waves in a channel with variable cross section,'' in Ref. 17, p. 87.
[19] M. H. Teng and T. Y. Wu, ''Nonlinear shallow water waves generated by submerged moving slender bodies: An experimental study,'' Proc. 7th Int. Offshore Polar Eng. Conf. **III**, 313 (1997).
[20] J. Mathew and T. R. Akylas, ''On three-dimensional long water waves in a channel with sloping sidewalls,'' J. Fluid Mech. **215**, 289 (1990).
[21] T. Y. Wu, ''A bidirectional long wave model,'' Methods Appl. Anal. **1**, 108 (1994).
[22] T. Y. Wu, ''Bidirectional soliton street,'' Acta Mech. Sinisa **11**, 289 (1995).
[23] M. H. Teng, ''Solitary waves in uniform channels with sloping sidewalls,'' submitted to Proc. R. Soc. London, Ser. A.